# Vibronic Spectroscopy of Methyl Anthranilate and its Water Complex: Hydrogen Atom Dislocation in the Excited State

| | |
|---|---|
| Journal: | *Physical Chemistry Chemical Physics* |
| Manuscript ID | CP-ART-08-2019-004556.R1 |
| Article Type: | Paper |
| Date Submitted by the Author: | 09-Sep-2019 |
| Complete List of Authors: | Blodgett, Karl; Purdue University, Department of Chemistry<br>Sun, Dewei; Purdue University, Department of Chemistry<br>Fischer, Joshua; Purdue University, Department of Chemistry<br>Sibert, Edwin L.; University of Wisconsin,<br>Zwier, Timothy; Purdue University, Department of Chemistry |
| | |

# Vibronic Spectroscopy of Methyl Anthranilate and its Water Complex: Hydrogen Atom Dislocation in the Excited State†

Karl N. Blodgett[a], Dewei Sun[a], Joshua L. Fischer[a], Edwin L. Sibert, III[b], and Timothy S. Zwier[a]*

[a]*Department of Chemistry, Purdue University, West Lafayette, Indiana 47907-2084, United States*

[b]*Department of Chemistry, University of Wisconsin-Madison, Madison, Wisconsin 53706, United States*

## Abstract

Laser-induced fluorescence (LIF) excitation, dispersed fluorescence (DFL), UV-UV-hole burning, and UV-depletion spectra have been collected on methyl anthranilate (MA, methyl 2-aminobenzoate) and its water-containing complex (MA-$H_2O$), under jet-cooled conditions in the gas phase. As a close structural analog of a sunscreen agent, MA has a strong absorption due to the $S_0$-$S_1$ transition that begins in the UV-A region, with the electronic origin at 28,852 $cm^{-1}$ (346.6 nm). Unlike most sunscreens that have fast non-radiative pathways back to the ground state, MA fluoresces efficiently, with an excited state lifetime of 27 ns. Relative to methyl benzoate, inter-system crossing to the triplet manifold is shut off in MA by the strong intramolecular NH···O=C H-bond, which shifts the $^3n\pi^*$ state well above the $^1\pi\pi^*$ $S_1$ state. Single vibronic level DFL spectra are used to obtain a near-complete assignment of the vibronic structure in the excited state. Much of the vibrational structure in the excitation spectrum is Franck-Condon activity due to three in-plane vibrations that modulate the distance between the $NH_2$ and $CO_2Me$ groups, $\nu_{33}$ (421 $cm^{-1}$), $\nu_{34}$ (366 $cm^{-1}$), and $\nu_{36}$ (179 $cm^{-1}$). Based on the close correspondence between experiment and theory at the TD-DFT B3LYP-D3BJ/def2TZVP level of theory, the major structural changes associated with electronic excitation are evaluated, leading to the conclusion that the major motion is a reorientation and constriction of the 6-membered H-bonded ring closed by the intramolecular NH···O=C H-bond. This leads to a shortening of the NH···O=C H-bond distance from 1.926 Å to 1.723 Å, equivalent to about a 25% reduction in the H···O distance compared to full H-atom transfer. As a result, the excited state process near the $S_1$ origin is a hydrogen atom dislocation that is brought about primarily by heavy atom motion, since the shortened H-bond distance results from extensive heavy-atom motion, with only a 0.03 Å increase in the NH bond length relative to its ground state value.

† Electronic supplementary information (ESI) available

*Author to whom correspondence should be addressed: zwier@purdue.edu

## I. Introduction

Methyl Anthranilate (MA) is the precursor to menthyl anthranilate (MenA), an FDA approved sunscreen agent.[1] Upon UV absorption, efficient sunscreen molecules are able to non-radiatively decay back to their ground electronic state, thereby regenerating their UV-absorbing capacities. In some cases, internal conversion is thought to be facilitated on the $S_1$ surface by H-atom transfer.[2-8] As such, much theoretical and experimental work has been directed toward understanding excited state hydrogen atom, or proton, transfer processes in this family of molecules. There are circumstances, however, in which excited state intramolecular H-atom transfer does not completely quench fluorescence, but instead leads to a Stokes-shifted fluorescence that signals its occurrence, as in the case of salicylic acid and methyl salicylate.[3, 4, 9, 10] This shifted emission provides a ready means of assessing the efficiency of the process as a function of vibrational level in the excited state.

For a hydrogen atom transfer process to occur, a donor hydrogen must be oriented toward an acceptor atom. Upon electronic excitation the donor X-H becomes more acidic while the acceptor Y becomes more basic, and the X-H bond is broken, resulting in the transfer of the hydrogen to the acceptor atom.[11, 12] In so doing, the excited state geometry rearranges as it moves on the potential energy surface, producing broad, red-shifted emission back to highly excited vibrational states in the ground state. This red-shifted emission is characteristic of these transient hydrogen transfer products. Alternatively, the excited state molecule may, through displacements along one or more internal coordinates, reach a conical intersection and non-radiatively decay back to the electronic ground state.[3, 11-13]

There is a body of evidence, however, that suggests that in some cases, rather than a complete hydrogen atom transfer, it is a hydrogen atom dislocation that occurs upon electronic excitation, where the X-H bond distance is increased, but not to the point of breaking and forming new covalent bonds.[14-19] In many ways, this is a fascinating circumstance in which the structural change on the excited state surface heads toward chemical reaction, but in not achieving it, enables detailed structural characterization. By dispersing the emission from the excited state vibrational levels, one observes the projection of each level back into the ground state in regions where the ground state vibrations still can be used as a set of modes to characterize the excited state structural change. In a previous study of the infrared (IR) and electronic spectroscopy of anthranilic acid and its water complex in the ground ($S_0$) and first excited ($S_1$) electronic states, the body of spectroscopic evidence pointed to a hydrogen atom dislocation, rather than transfer, occurring upon electronic excitation.[14, 15] However, no dispersed fluorescence scans were carried out, limiting the degree to which structural characterization was possible.

In the present study, we carry out just such a study on a close analog of anthranilic acid, methyl anthranilate, which replaces the carboxylic acid hydrogen with a methyl group. MA, shown in **Figure 1**, has a 6-membered hydrogen bonded ring closed by an NH···O=C H-bond. In this first of two papers on MA, we report a detailed study of the vibrationally-resolved electronic spectroscopy of MA and its single-water complex, MA-$H_2O$, in both the ground and excited electronic states. Using a suite of laser-based techniques, coupled with density functional theory calculations, we interrogate the vibronic structure of jet-cooled MA and MA-$H_2O$, and extract and discuss the structural implications of the spectra.

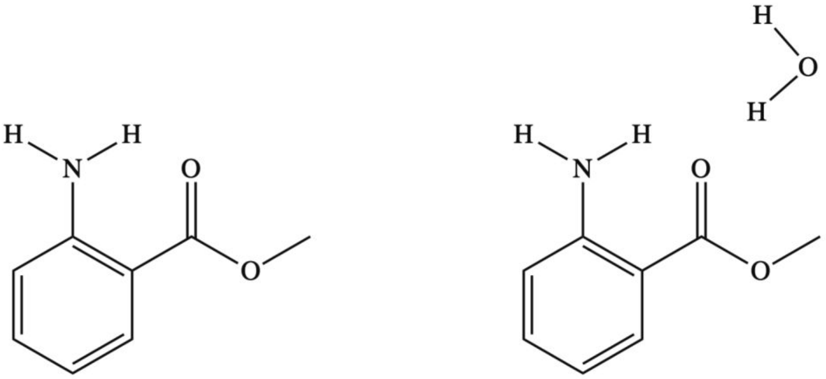

**Figure 1:** Chemical structures of methyl anthranilate (MA) and methyl anthranilate-water complex (MA-$H_2O$).

## II. Experimental and Computational Methods

Methyl anthranilate was purchased from Sigma-Aldrich (≥99% purity) and used without further purification. The instrument used to collect fluorescence data has been described in detail elsewhere.[20] The sample was entrained in 2.0 bar backing pressure of helium and expanded through an 800 μm orifice of a pulsed valve (Parker series 9 General valve) into a vacuum chamber pumped by a roots blower. In the ensuing supersonic expansion, collisions with the helium backing gas serve to cool MA to its ground state zero-point vibrational energy level. The MA-$H_2O$ complex was observed in the expansion without changing experimental conditions, formed by residual $H_2O$ present in the lines and sample. The identity of the MA monomer and water complex were verified by mass-resolved excitation spectra (see **SI Section 1**). The collisionally cooled molecules are interrogated by one or more lasers propagating perpendicular to the expansion, intersecting the expansion approximately 8 mm downstream from the source. Emission is collected at the focal point of two 4-inch diameter spherical mirrors, the bottom of which has a 1 cm hole through which resonant fluorescence is steered. This light is collimated through a plano-convex lens, passed through long-pass filters to reduce scattered laser light, and imaged onto a photomultiplier tube. Laser induced fluorescence (LIF) excitation spectra were collected by scanning the output of a 20 Hz frequency doubled Nd:YAG-pumped dye laser (Radiant Dyes NarrowScan) across the 28,500-30,000 $cm^{-1}$ region associated with the $S_0$-$S_1$ transition of MA, where total collected fluorescence is plotted as a function of excitation wavelength.

Since the LIF spectrum contains contributions from all possible conformational isomers (conformers) and complexes of MA, double resonance laser techniques were employed to decompose the spectrum into its component parts. UV-UV holeburning (UV-UV HB), IR-UV holeburning (IR-UV HB), and UV depletion (UV-D) spectroscopies were used for this purpose. In UV-UV HB, a 10 Hz hole-burn laser (Lambda Physik Scanmate) has its wavelength fixed on some vibronic transition in the LIF spectrum. This hole-burn laser temporally precedes by 100 ns, a 20 Hz probe laser which is scanned through the region of interest. When the probe laser wavelength is resonant with a vibronic transition which shares the same ground state as the transition on which the hole-burn laser is fixed, a decrease in fluorescence results from the depletion of ground state zero-point populated molecules. This difference is measured by passing the 20 Hz fluorescence signal through a gated integrator operating in active baseline subtraction mode, the output of which is equivalent to a conformer- or complex-specific UV excitation spectrum. IR-UV HB is the same as UV-UV HB, except that the 10 Hz hole-burn laser is now an IR laser (LaserVision OPO) which has its frequency fixed on a unique vibrational transition of the species of interest.

UV-D is similar to UV-UV HB, except that the 10 Hz hole-burn laser is scanned through the region of interest, while the 20 Hz probe laser is fixed on some vibronic transition, whose constant fluorescence signal is monitored. As in UV-UV HB, a conformer-specific UV spectrum is generated. The UV-D spectrum has the advantage that it enables acquisition of the true absorption spectrum, regardless of whether the tuned HB laser accesses states that fluoresce appreciably or not. In this experimental scheme, the signal is a ground state depletion, which is governed solely by the absorption properties of the molecule, rather than the modulation of excited state-dependent fluorescence. Comparison of the UV-D to the UV-UV HB spectrum gives insight into the nature and extent of non-radiative processes that may occur in the excited state. A disadvantage of the method is that the UV-D spectrum measures depletion of a constant non-zero signal, and therefore has the inherent noise associated with subtraction of two large signals.

Dispersed fluorescence (DFL) spectra were used to aid in the assignment of the transitions in the excitation spectrum by resolving the emission from individual excited state levels prepared by the laser. In this scheme, an excitation laser has its wavelength fixed on some vibronic transition of interest. The emitted fluorescence is dispersed by passing it through a ¾-meter monochromator outfitted with a grating blazed for UV detection. The dispersed emission is then imaged at the output focal plane onto a gated-intensified CCD camera. This technique determines the ground state vibrational levels formed by emission from a single, laser-prepared excited state vibrational level.

Conformational searches of MA and MA-$H_2O$ were performed using a torsional-sampling Monte Carlo Multiple Minimum algorithm with the OPLS3 force field within the MacroModel computational suite. These calculated structures served as the starting structures for geometry optimization via density functional theory (DFT) calculations, using the Becke 3LYP (B3LYP) hybrid functional supplemented with the D3 version of Grimme's dispersion correction[21] and Becke-Johnson (BJ) damping.[22] This functional was used in conjunction with the def2TZVP basis set to calculate harmonic vibrational frequencies of the optimized ground state structures. Time dependent DFT (TD-DFT) calculations were then used to calculate vertical and adiabatic excitation energies as well as the geometry and harmonic vibrational frequencies of the first excited singlet state of multiple MA and MA-$H_2O$ conformers. The Gaussian16 suite of programs was used for the DFT calculations and the visualization of normal modes.[23] Molecular orbitals and optimized structures were visualized using the Gaussian16 suite and Chemcraft Software.[24]

## III. Results and Analysis

### A. Methyl Anthranilate Monomer

## 1. Computational Predictions

In its ground state, MA may exist as either of two rotamers: one where the amine group hydrogen bonds with the ester oxygen, and the other in which the amine group hydrogen bonds with the carbonyl oxygen (see **Figure S2**). At the DFT B3LYP-D3BJ/def2TZVP level of theory, the second rotamer is calculated to be 13.3 kJ/mol lower in energy than the first rotamer. In the supersonic free jet environment, one would anticipate all of the population funneling to the lower energy rotamer. Key structural parameters predicted by the calculations for the C=O bound rotamer in the ground ($S_0$) and first excited ($S_1$) singlet states are shown in **Figure 2**. The $S_1$ geometry is predicted to be planar, while the $S_0$ equilibrium geometry deviates slightly from planarity along the $NH_2$ inversion coordinate. Relaxed potential energy scans performed along the CNHH improper dihedral angle reveal a wide symmetric double minimum potential in the $S_0$ electronic state with minima at ±18° and a tiny 5 $cm^{-1}$ inversion barrier centered at the planar geometry (see **Figure S3**). Since this barrier is well below the zero-point energy, we should anticipate a quasi-planar $S_0$ geometry with a vibrationally averaged planar configuration, with no inversion tunneling splitting.

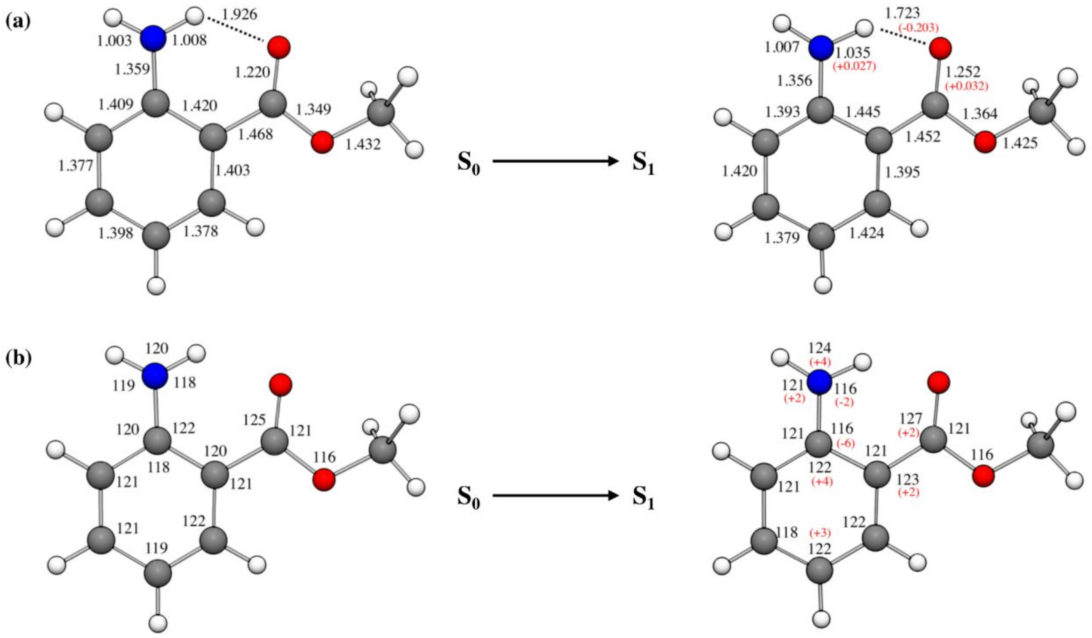

**Figure 2:** Optimized ground and $S_1$ excited state geometries of MA with (a) bond distances and (b) bond angles labelled. Bond lengths are in angstroms (Å) and angles are in degrees. The difference between select ground and excited state parameters are shown in red parentheses. Values were calculated at the DFT B3LYP-D3BJ/def2TZVP level of theory.

Since both the $S_0$ and $S_1$ geometries have one mirror plane, they both belong to the $C_s$ point group. As such, the 54 normal modes reduce to 36 totally symmetric (a′, in-plane) and 18 non-totally symmetric (a′′, out-of-plane) vibrations. Symmetry also constrains the vibronic transitions. According to electric dipole selection rules within the Franck-Condon approximation, allowed transitions originating from the zero-point level include the fundamentals of all in-plane vibrations and only even combinations of out-of-plane vibrations via overtones or combination bands. It is worth noting that intensity in combination bands depends on Duschinsky mode mixing for their intensity.[25] In this manuscript, we use Mulliken notation[26] to describe and order the normal modes of vibration.

Vertical TD-DFT B3LYP-D3BJ/def2TZVP calculations predict that the $S_1$ electronic state is optically accessible from $S_0$ via a $\pi\pi^*$ electron transition with contributions from HOMO → LUMO and (HOMO-1) → (LUMO+1) transitions. This $S_0$-$S_1$ transition has an appreciable oscillator strength ($f_{01} = 0.1036$). Furthermore, the $S_1$ state is well isolated from other excited states, with $S_2$ and $S_3$ 1.15 and 1.30 eV above $S_1$ (see **Section S4** for molecular orbital transitions in MA). Due to the large energy separation between $S_1$ and $S_2$/$S_3$, and smaller oscillator strengths from $S_0$, one would not anticipate significant manifestations of vibronic coupling in the $S_0$-$S_1$ vibronic spectrum.

### 2. UV Excitation Spectroscopy

The LIF excitation spectrum of MA is presented in **Figure 3a**. The spectrum spans from 28,825 - 30,000 cm$^{-1}$ (346.9-333.0 nm), with the $S_0$ - $S_1$ electronic origin transition appearing at 28,852 cm$^{-1}$. The lifetime of the $S_1$ state is measured to be 27 ns (see **Figure S8a** for the fluorescence decay trace). **Figure 3b** shows the UV-UV HB spectra of MA, recorded with the HB laser fixed on the transition at 28,852 cm$^{-1}$. This spectrum shows that the majority of the peaks in the LIF excitation spectrum are due to the MA monomer. This assignment was verified via mass-resolved two-color resonant two-photon ionization (2C-R2PI) excitation spectra (see **Figure S1a**). The minor peaks in the LIF spectrum that do not burn out in the UV-UV HB scan belong to the MA-$H_2O$ complex (discussed in detail in section B). To distinguish whether the decrease in intensity in the spectra with increasing excitation energy is due to the drop-off in Franck-Condon factors or some non-radiative decay process, we collected UV-D spectra, shown in **Figure 3c**. The UV-D spectrum contains the same peaks and intensity pattern as the UV-UV HB spectra. This indicates that, in the wavelength region we have probed, there is no turn-on of a non-radiative process at play, and that the intensities in the LIF and UV-UV HB spectra presented in **Figure 3a** and **3b** are determined primarily by the absorption properties of MA.

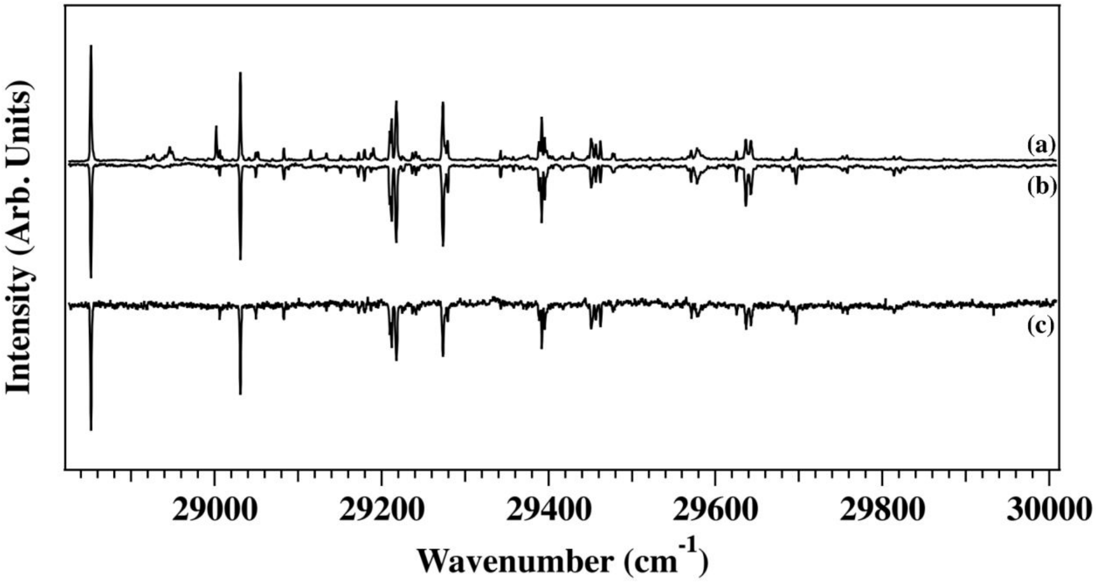

**Figure 3:** (a) LIF excitation, (b) UV-UV hole-burning, and (c) UV depletion spectra of MA from 28,825 - 30,000 cm$^{-1}$.

The assigned IR-UV HB spectrum of MA is displayed in **Figure 4**. These assignments were reached based on corroborating evidence from $S_0$ and $S_1$ vibrational frequency calculations, excitation spectra, and DFL spectra, as will be discussed in detail below. A rotational band contour (RBC) scan of the electronic origin transition, taken at a laser resolution of 0.15 cm$^{-1}$ (in the UV) is shown as the top trace in **Figure S9**. Using the spectral fitting program JB95[27], along with transition dipole moment (*a:b:c* = 77:23:0) components and rotational constants from the calculated ground and excited states, we obtained the simulated RBC shown as the bottom trace in **Figure S9**. The excellent match between experiment and theory bolsters the assignment of MA to the lower energy rotamer.

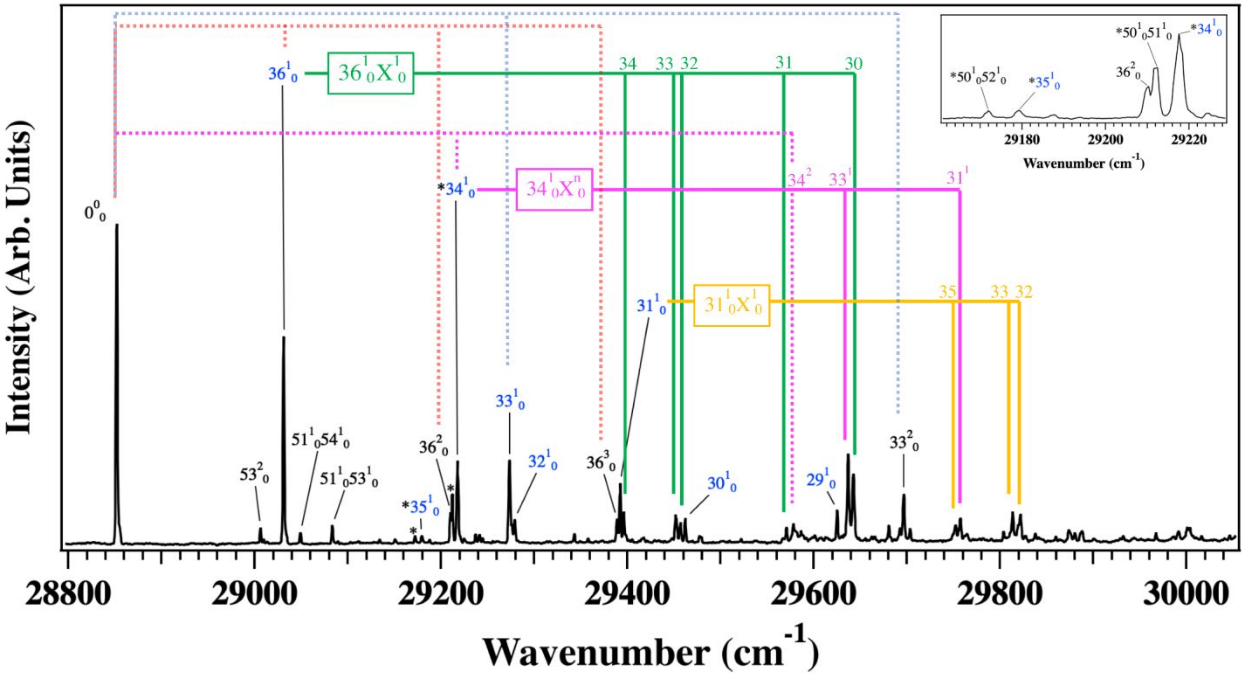

**Figure 4:** Assigned $S_0$ - $S_1$ LIF excitation spectrum of MA. Progressions in the in-plane modes $\nu_{36}$ (179 cm$^{-1}$), $\nu_{34}$ (366 cm$^{-1}$), and $\nu_{33}$ (421 cm$^{-1}$) are m via red, pink, and blue dotted tie-lines, respectively, while in-plane combination bands built off $36^1_0$, $34^1_0$, and $31^1_0$ are shown with solid tie lines. The identity of mode X is listed above each respective tie line. The inset provides a close-up view of the two pairs of peaks identified as Fermi-resonance pairs.

**Table 1** lists the type experimental and calculated $S_0$ and $S_1$ vibrational frequencies. The excitation spectrum of MA is composed of progressions in in-plane vibrations, even combination bands and overtone transitions of out-of-plane vibrations, and (1+1):1 Fermi resonance pairs between out-of-plane combination bands and in-plane fundamentals. Progressions in the in-plane modes $\nu_{36}$ (179 cm$^{-1}$), $\nu_{34}$ (366 cm$^{-1}$), and $\nu_{33}$ (421 cm$^{-1}$) are displayed via red, pink, and blue dotted tie-lines, respectively, while in-plane combination bands built off $36^1_0$, $34^1_0$, and $31^1_0$ are shown with solid tie lines. All other assigned peaks, belonging either to in-plane fundamentals or out-of-plane combination bands, are labelled with tags.

It is noteworthy that, while the $0^0_0$ transition is the largest peak in the spectrum, all eight of the lowest frequency in-plane fundamentals ($\nu_{36\text{-}29}$) have measurable intensity in their $X^1_0$ fundamentals, indicating a geometry change along these normal coordinates between the ground and excited electronic states. The two pairs of peaks designated with asterisks (and shown in the figure inset) are identified as Fermi-resonance pairs. The five lowest frequency out-of-plane modes, $\nu_{54-50}$, appear as combination and, in the case of $\nu_{53}$, overtone bands.

**Table 1: Experimental and Calculated $S_0$ and $S_1$ Frequencies of MA, Best Fit Normal Coordinate Displacement Values, and Excited to Ground State Normal Mode Projections**

| $S_0$ | | | $S_1$ | | | |
|---|---|---|---|---|---|---|
| a' In-Plane Modes | | | | | | |
| Mode | Exp Freq (cm$^{-1}$) | Calc Freq[a] (cm$^{-1}$) | Exp Freq (cm$^{-1}$) | Calc Freq[a] (cm$^{-1}$) | Best-Fit Displacement[b] | $S_1 \rightarrow S_0$ mode projections[c] |
| 36 | 179 | 183 | 179 | 183 | 0.97 | 33,31,29 |
| 35 | 333 | 340 | 327 | 333 | 0.10 | |
| 34 | 361 | 359 | 366 | 364 | 0.85 | 36,33,31,29 |
| 33 | 412 | 420 | 421 | 423 | 1.27 | 36,34,31,29 |
| 32 | 494 | 506 | 427 | 502 | 0.50 | 36, 33, 31, |
| 31 | 567 | 574 | 540 | 559 | 0.60 | 33, 30 |
| 30 | 672 | 684 | 610 | 641 | 0.10 | 29 |
| 29 | 808 | 818 | 773 | 786 | 0.50 | 33 |
| 18 | 1355 | 1353 | - | 1381 | - | - |
| a'' Out of Plane Modes | | | | | | |
| Mode | Exp Freq (cm$^{-1}$) | Calc Freq (cm$^{-1}$) | Exp Freq (cm$^{-1}$) | Calc Freq (cm$^{-1}$) | Best-Fit D | $S_1 \rightarrow S_0$ mode projections |
| 54 | 57 | 65 | 44 | 49 | 0 | 51,52,53 |
| 53 | 96 | 97 | 77 | 82 | 0 | 51,53,54 |
| 52 | 143 | 145 | 114 | 117 | 0 | 50,51 |
| 51 | 161 | 163 | 153 | 156 | 0 | 50,52,53,54 |
| 50 | 229 | 254 | 207 | 220 | 0 | 51,52 |

[a] Frequencies calculated at the DFT B3LYP-D3BJ/def2TZVP level of theory. [b] Value calculated using the Franck-Condon fitting procedure discussed in **Section S15**. [c] Determined from DFL data

### 3. DFL of the $0^0_0$ Band and In-Plane Fundamentals

The assigned DFL spectrum of the electronic origin transition is shown in **Figure 5**. The peak positions and intensity pattern displayed in the first 1,200 cm$^{-1}$ of the DFL spectrum largely mirror those of the excitation spectrum, as would be the case if Franck-Condon factors between the ground and excited state play a dominant role in the observed vibronic structure. This DFL spectrum shows progressions in three in-plane modes; $\nu_{36,}$ $\nu_{34,}$ $\nu_{33,}$ all of which also showed clear progressions in the excitation spectrum. Additionally, each in-plane fundamental that we observe in the excitation spectrum appears with an analogous $\Delta\nu=1$ transition in the origin DFL spectrum, with one additional higher frequency band appearing at +1355 cm$^{-1}$ ($\nu_{18}$). As was the case with the excitation spectrum, we also observe in-plane and out-of-plane combination bands and out-of-plane overtones in the DFL spectrum. The DFL spectrum also has a large number of in-plane combination bands, with a smaller number of out-of-plane combination bands.

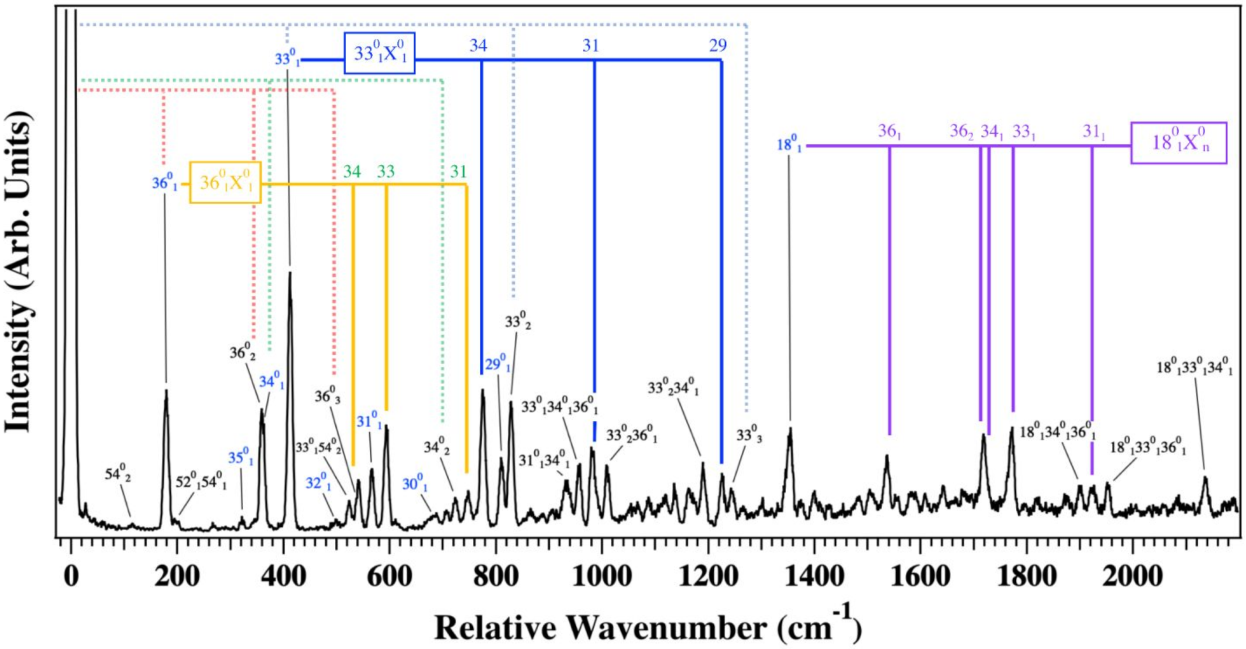

**Figure 5:** Dispersed fluorescence spectrum of the $S_0$ - $S_1$ origin transition of MA. Progressions in the in-plane modes $\nu_{36}$ (179 cm$^{-1}$), $\nu_{34}$ (361 cm$^{-1}$), and $\nu_{33}$ (412 cm$^{-1}$) are displayed via red, green, and blue dotted tie-lines, respectively, while in-plane combination bands built off $36^1_0$, $33^1_0$, and $18^1_0$ are shown with solid tie lines. The identity of mode X is listed above each respective tie line.

**Figure 6** presents the DFL spectra of the eight Franck-Condon active in-plane fundamentals present in the excitation spectrum. In the +327 cm$^{-1}$ DFL spectrum **(Figure 6b)** there is a large peak at 333 cm$^{-1}$ with no further progressions at that frequency. The majority of the remainder of the peaks built off of this transition, labelled with red dotted tie lines, are identical in relative frequency and intensity pattern to the entire set of peaks in the $0^0_0$ DFL spectrum, indicating that the 333 cm$^{-1}$ peak serves as a false origin (labelled with a red $0^0_0$ in **Figure 6**). The strong intensity of the peak at 333 cm$^{-1}$, combined with the excellent agreement between calculated and experimental frequency, leads us to assign the +327 cm$^{-1}$ transition to the $35^1_0$ in-plane

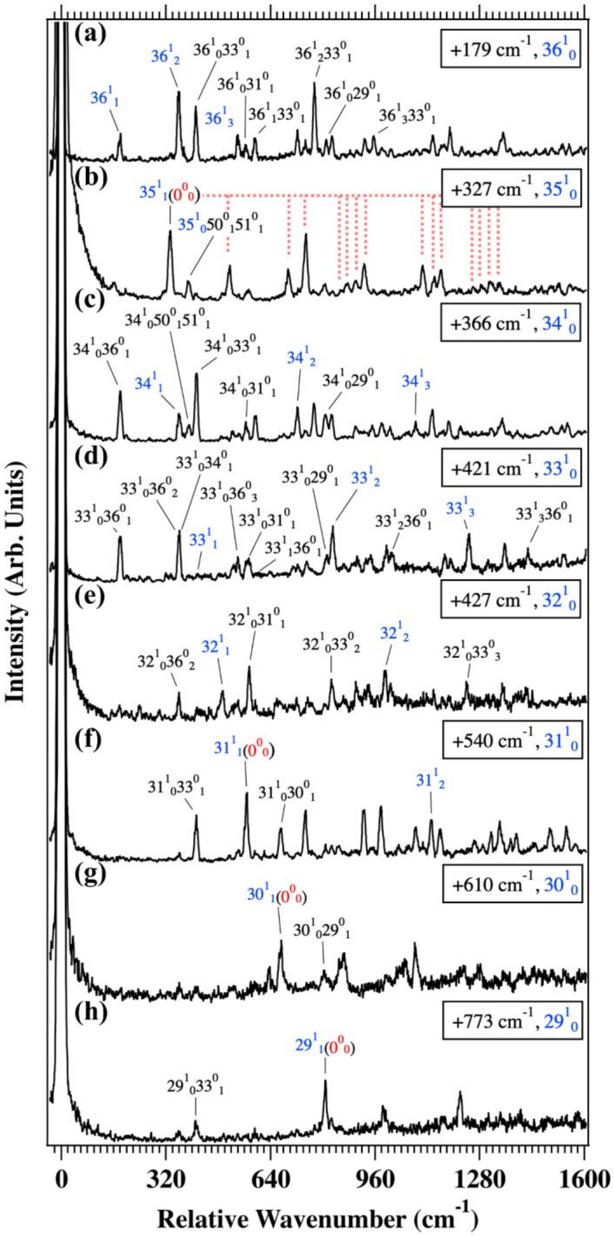

**Figure 6:** DFL spectra of the Franck-Condon active, in-plane fundamentals in MA: (a) $36^1_0$, (b) $35^1_0$, (c) $34^1_0$, (d) $33^1_0$, (e) $32^1_0$, (f) $31^1_0$, (g) $30^1_0$, and (h) $29^1_0$. Ground state progressions in analogous modes are labelled in blue text, and transitions which serve as false origins are marked with a red ($0^0_0$).

fundamental, and the 333 cm$^{-1}$ peak as a Δv=0 transition ($35^1_1$). The intensity pattern this mode displays in the vibronic spectra, together with the $35^1_1$ transition serving as a false origin, indicate a very small displacement of its respective potential wells between $S_0$ and $S_1$ states. The

$\Delta\nu=0$ transition of several other excited state modes, $\nu_{31}$, $\nu_{30}$, $\nu_{29}$ (**Figure 6f-h**), also serve as false origins involving each of these vibrations.

Many of these DFL spectra contain, among other transitions, progressions in their analogous ground state normal mode (labelled in blue in **Figure 6**). The DFL spectrum of the transition at +179 cm$^{-1}$, for example, displays a Franck-Condon progression in a 179 cm$^{-1}$ mode in $S_0$. Based on the extent of the Franck-Condon activity in the excitation and $0^0_0$ DFL spectra in 179 cm$^{-1}$, one should expect concomitant progressions in the ground state when projecting from $\nu=1$ in $S_1$. This evidence, in addition to the agreement between calculated and experimental frequencies, leads us to assign the +179 cm$^{-1}$ transition in the excitation spectrum to the $36^1_0$ in-plane fundamental. The long progressions in the vibronic spectra of $\nu_{36}$ (with $36^1_n$ members up through n=3) implies an appreciable displacement of the respective normal mode coordinates upon electronic excitation.

This one-dimensional normal coordinate displacement, however, does not account for all of the peaks in the $36^1_0$ DFL spectrum. There are also several cross-sequence bands present, most notably $36^1_n33^0_1$, $36^1_031^0_1$ and $36^1_029^0_1$. Such cross-sequence bands are signatures of Duschinsky mixing, in which the normal coordinates in the $S_1$ state are linear combinations of the ground state normal coordinates.[28] This may be thought of as a rotation of the normal coordinates on the $S_1$ potential energy surface (PES) relative to the $S_0$ PES, where the one-to-one correspondence between ground and excited state normal modes is lost to some degree.[29] The situation is further complicated for in-plane modes, where, in addition to mixing, displacements along the normal coordinate(s) may occur. We may deduce, then, via its Franck-Condon activity and cross-sequence bands, that the $\nu_{36}$ coordinate in $S_1$ is both rotated and its origin displaced relative to its corresponding coordinate in $S_0$.

The prevalence of cross-sequence bands in the in-plane fundamental DFL spectra presented in **Figure 6** implies a significant degree of Duschinsky mixing upon electronic excitation. Using similar logic as that outlined above, we have assigned nearly all of the transitions in the excitation and DFL spectra. Confidence in these assignments is bolstered by the strong agreement between calculated and experimentally assigned vibrational frequencies (**Table 1**). **Figure 7** shows the ground state form of the Franck-Condon active in-plane normal modes.

Based on the Franck-Condon activity, the largest displacements are in modes 36 (179 cm$^{-1}$) and 33 (421 cm$^{-1}$), similar to what is observed in anthranilic acid.[15]

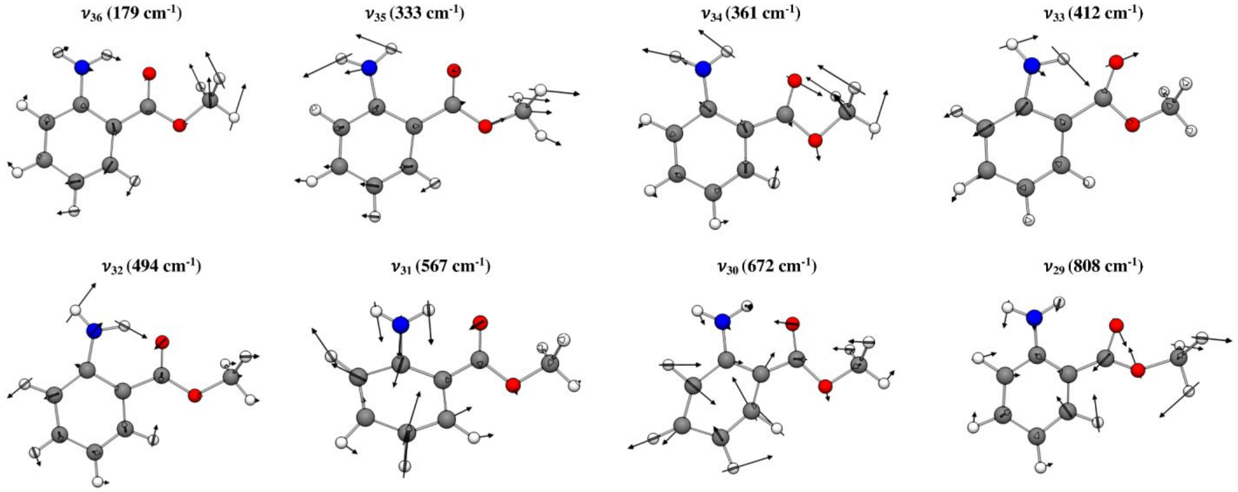

**Figure 7:** Ground state in-plane normal modes $\nu_{36}$–$\nu_{29}$ of MA. Normal modes were calculated at the DFT B3LYP-D3BJ/def2TZVP level of theory.

Through the DFL spectra, we were also able to identify the onset of intramolecular vibrational energy redistribution (IVR) in the $S_1$ state. IVR results when the laser-prepared state carrying the oscillator strength in excitation anharmonically couples with a bath of background states at that energy. This bright state/background state mixing of the upper state wave function has the effect of taking what would be sharp vibronic transitions and broadening/shifting transitions due to the state's background character. **Figure S10** presents a sequence of DFL spectra taken at increasing energies relative to the origin. At pump energies greater than 600 cm$^{-1}$ we note the appearance of a broad, increasing baseline, most likely associated with the onset of IVR. The spectral signature of IVR is less clear in the context of MA than it is in many phenyl derivatives[30, 31], due to the much larger geometry change between $S_0$ and $S_1$ in MA.

### 4. DFL of the Out-Of-Plane Combination Bands and Fermi Resonance Pairs

The assigned DFL spectra of the transitions assigned to out-of-plane modes are shown in **Figure 8**. It is noteworthy that all assigned transitions involve even overtone and combination bands in the out-of-plane modes, providing convincing experimental evidence that the molecule retains $C_s$ symmetry in both ground and excited states. Whereas in-plane modes may undergo both mixing and displacement upon electronic excitation in systems where $C_s$ symmetry is preserved in both states, out-of-plane modes have zero displacement of normal coordinates upon excitation. This zero displacement results in transitions involving out-of-plane modes having weak intensity in the excitation or $0^0$ DFL spectra.

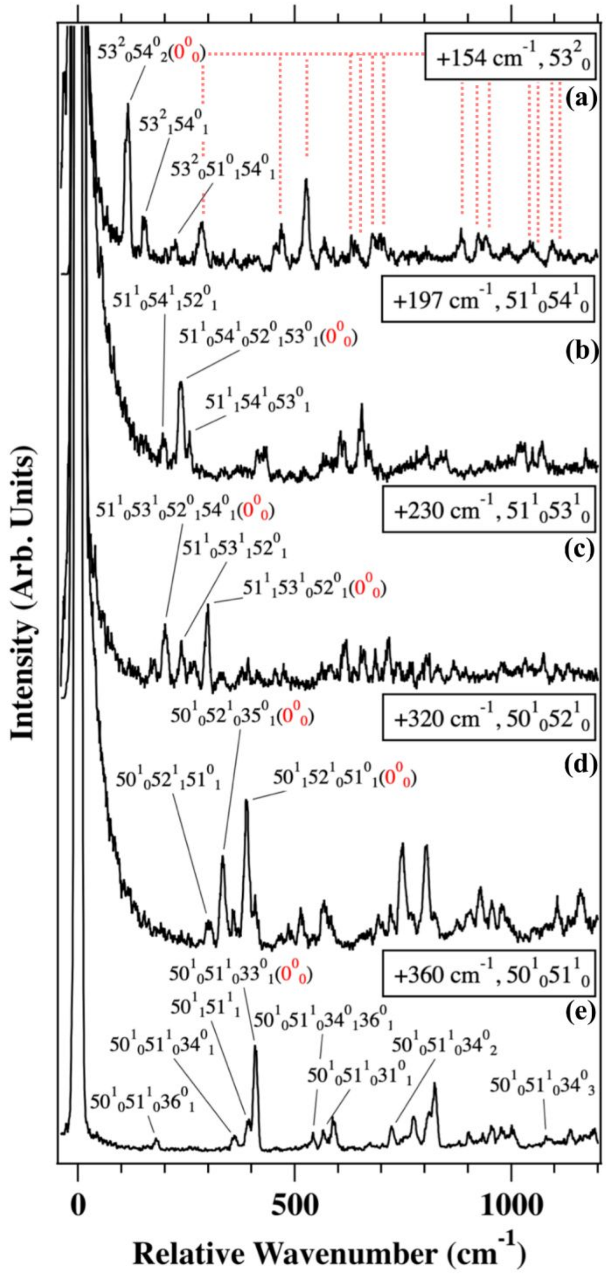

**Figure 8:** DFL spectra of transitions involving out-of-plane modes in MA: (a) $53^2_0$, (b) $51^1_0 54^1_0$, (c) $51^1_0 53^1_0$, (d) $50^1_0 52^1_0$, and (e) $50^1_0 51^1_0$. Transitions which serve as false origins are marked with a red $(0^0_0)$.

In all of the DFL spectra in **Figure 8** there are strong bands in the low frequency region that serve as false origins for transitions built off of them; that is, one can readily assign Franck-Condon activity built off these transitions that mirror the Franck-Condon activity present in the $0^0$ DFL spectrum **(Figure 5).** It is noteworthy that, in all the spectra in **Figure 8**, the most intense false origin is not the Δv=0 transition (e.g., $X^1{}_1Y^1{}_1$ following excitation of $X^1{}_0Y^1{}_0$) but instead, one or more cross-sequence band(s).

The abundant cross-sequence transitions assigned in **Figure 8** indicate extensive Duschinsky mixing among the out-of-plane modes. **Figure 9** shows the form of these normal modes in the ground state, along with the reduced Duschinsky rotation matrix calculated at the B3LYP-D3BJ/def2TZVP level of theory. The matrix elements across a row (non-negligible off-diagonal components highlighted in blue) give the expansion coefficients of the indicated $S_1$ normal coordinate in terms of the $S_0$ coordinates. Without direct data on cross-sequence hot bands of the type $X^1{}_0Y^0{}_1$, it is difficult to carry out quantitative tests of the Duschinsky mixing[29, 32]. Nevertheless, we can use this matrix to see whether it is qualitatively consistent with the experimental data; that is, by looking at which modes show clear evidence of mixing with one another. For example, the largest peak in the $53^2{}_0$ DFL spectrum is the cross-sequence band $53^2{}_0 54^0{}_2$, consistent with the large off-diagonal mixing (-0.230) between these two modes. Indeed, DFL spectra from levels with excitation in modes 52, 53, and 54 show significant mixing between all three, as the Duschinsky matrix predicts.

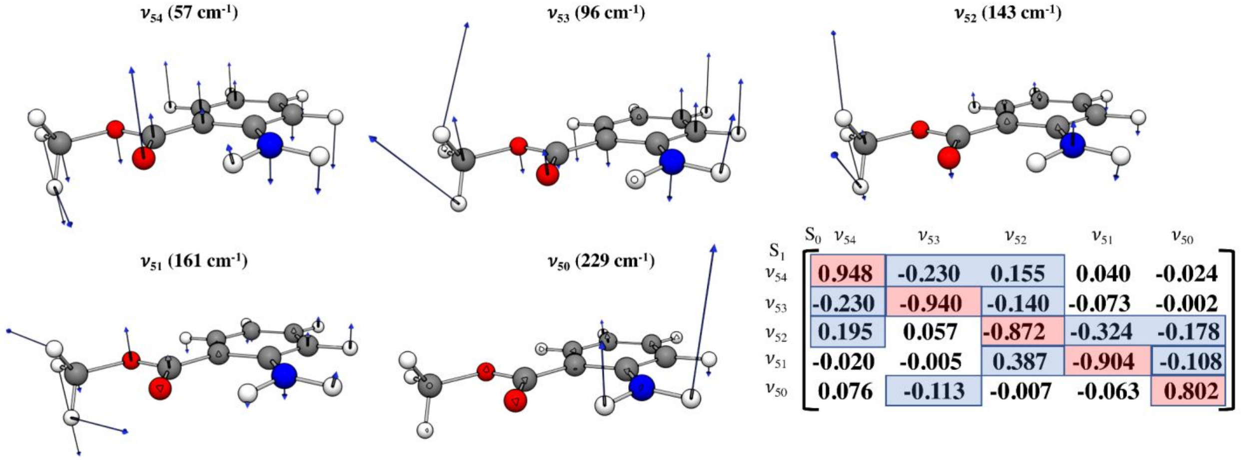

| $S_1$ \ $S_0$ | $\nu_{54}$ | $\nu_{53}$ | $\nu_{52}$ | $\nu_{51}$ | $\nu_{50}$ |
|---|---|---|---|---|---|
| $\nu_{54}$ | **0.948** | **-0.230** | **0.155** | **0.040** | **-0.024** |
| $\nu_{53}$ | **-0.230** | **-0.940** | **-0.140** | **-0.073** | **-0.002** |
| $\nu_{52}$ | **0.195** | **0.057** | **-0.872** | **-0.324** | **-0.178** |
| $\nu_{51}$ | **-0.020** | **-0.005** | **0.387** | **-0.904** | **-0.108** |
| $\nu_{50}$ | **0.076** | **-0.113** | **-0.007** | **-0.063** | **0.802** |

**Figure 9:** Ground state out-of-plane normal modes $\nu_{54}$–$\nu_{50}$ of MA, along with the reduced Duschinsky matrix of these modes. The matrix row elements give the expansion coefficients of the indicated $S_1$ normal coordinate in terms

of the $S_0$ coordinates. The normal modes and Duschinsky matrix were calculated at the DFT B3LYP-D3BJ/def2TZVP level of theory.

The spectra in **Figure 8d,e** show strong false origins in bands that cannot be understood purely in terms of Duschinsky mixing. Indeed, as the inset in **Figure 4** shows, in the excitation spectrum, the $50^1_0 52^1_0$ and $50^1_0 51^1_0$ transitions appear in close proximity with the in-plane fundamentals $35^1_0$ and $34^1_0$, respectively, marked with asterisks. The first set of peaks are assigned to the $50^1_0 52^1_0$ combination and Franck-Condon allowed $35^1_0$ fundamental transitions. The DFL spectra coming out of this pair (shown in **Figures 10a, b**) provide evidence that they are in Fermi-resonance with one another. These spectra share almost all of the same transitions to the ground state, thus revealing their mixed character in the excited state. To substantiate this claim, consider the $50^1_0 52^1_0 35^0_1$ transition in the $50^1_0 52^1_0$ DFL spectrum. The excitation spectrum (**Figure 4**), origin and $35^1_0$ DFL spectra (**Figure 5** and **6b**) all show that $\nu_{35}$ has

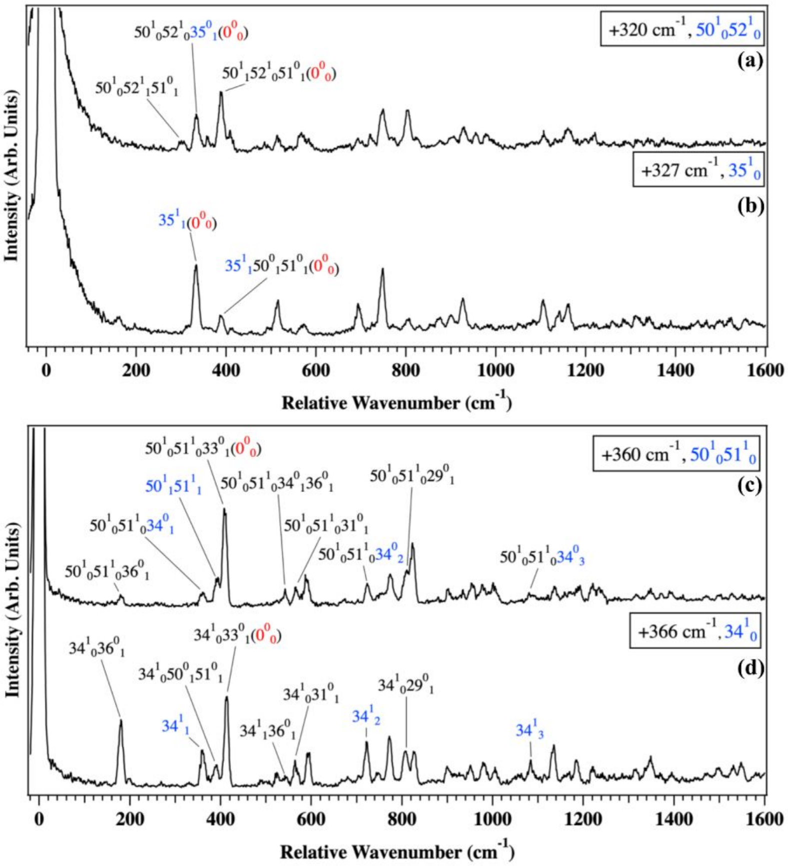

**Figure 10:** DFL of Fermi resonance modes (a) $50^1_0 52^1_0$ and (b) $35^1_0$, and (c) $50^1_0 51^1_0$ and (d) $34^1_0$ of MA. Ground state transitions to Fermi-mixed components are labelled in blue text, and transitions which serve as false origins are marked with a red ($0^0_0$).

essentially no oscillator strength in its Δν=1 transitions. The substantial intensity of this transition in the $50^1_0 52^1_0$ DFL spectrum, then, implies that the upper state contains some $35^1$ character. Furthermore, the lack of a Δν=0 $50^1_1 52^1_1$ transition in either DFL spectrum, but the corresponding presence of a $50^1_1 51^1_1$ transition in both, implies strong Duschinsky mixing between modes 51 and 52, as predicted by the Duschinsky matrix in **Figure 9**.

The second set of peaks is assigned to an excited state Fermi resonance between the $50^1 51^1$ combination level and the $34^1$ in-plane fundamental. The DFL spectra coming out of these levels is shown in **Figure 10c** and **10d**, respectively. The presence of Fermi resonant mixing between the pair of excited state levels is manifested by the Δv=0 emission to both the $50_1 51_1$ and $34_1$ ground state levels appearing in both DFL spectra. Oddly enough, the $50^1_1 51^1_1$ transition is the only observed case in which a fully Δv=0 transition is even observed in the DFL spectra of these out-of-plane combination levels. Nonetheless, the presence of this Δv=0 transition has enabled a quantitative analysis of the Fermi resonance mixing coefficients, $\alpha$ and $\beta$ with $\alpha$=0.802 and $\beta$=0.597. Using these expansion coefficients, the calculated Franck-Condon integrals reproduce, with high fidelity, the relative peak intensities observed in the DFL spectra. See **Section S8** for details.

## B. Methyl Anthranilate-Water Complex

### 1. Computational Predictions

Complexation of a single water molecule to MA (MA-$H_2O$) can occur at several binding sites, supporting numerous conformers. At the DFT B3LYP-D3BJ/def2TZVP level of theory we have calculated seven minima lying within 10 kJ/mol of the global energy minimum (see **Figure S13** and **Table S1**). In each of these structures, the monomer portion adopts the same rotamer form that we have just assigned, i.e., with the amine group hydrogen bonded with the carbonyl group. None of the conformers have symmetry in their calculated $S_0$ or $S_1$ states. This is not due, as was the case in the MA $S_0$ geometry, to a symmetric double well potential along the $NH_2$ inversion coordinate, but rather the $H_2O$ molecule asymmetrically binding to the MA monomer unit with an out-of-plane position for its center-of-mass. The calculated equilibrium structure of the assigned MA-$H_2O$ complex in its $S_0$ and $S_1$ geometry is shown in **Figure 11**. This conformer was calculated to be the zero-point corrected energy minimum both with and without basis set superposition error (BSSE) correction (see **Figure S13** and **Table S1)**.

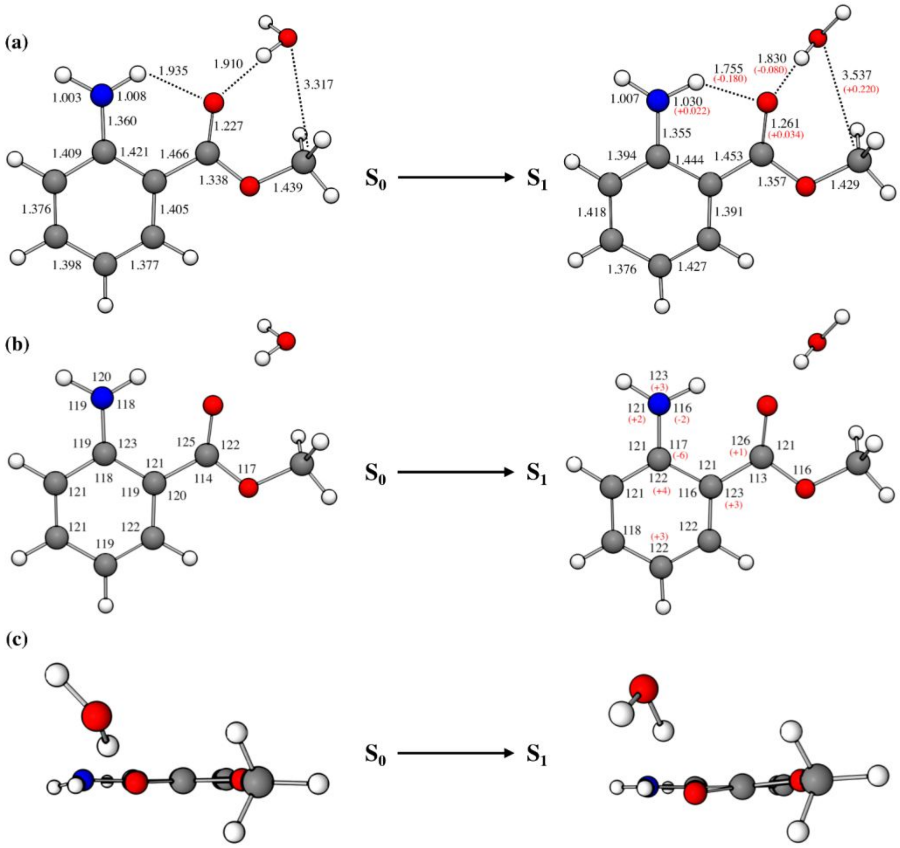

**Figure 11:** Optimized ground and $S_1$ excited state geometries of MA-$H_2O$ with (a) bond distances and (b) bond angles labelled, and (c) a side view showing the change in water position upon electronic excitation. Bond lengths are in angstroms (Å) and angles are in degrees. The difference between select ground and excited state parameters are shown in red parentheses. Values were calculated at the DFT B3LYP-D3BJ/def2TZVP level of theory.

The loss of symmetry upon water complexation means that the in-plane/out-of-plane selection rules present in MA monomer are no longer present in the complex. As we shall see, however, the relative intensities of certain bands in the excitation spectrum suggest a weakening of these selection rules rather than a binary switch between on and off. The 63 normal modes of vibration of the complex are designated with the Mulliken scheme, from high to low frequency. Nevertheless, many of the MA vibrations retain much of their character upon water complexation, and we refer to this connection in what follows. Formally speaking, six new intermolecular vibrations are associated with hindered translation (3) and rotation (3) of the $H_2O$ molecule relative to MA.

Vertical TD-DFT B3LYP-D3BJ/def2TZVP calculations predict that the $S_1$ electronic state of MA-$H_2O$ is very similar to its character in MA monomer, with a nearly-identical form for the molecular orbitals and their coefficients in the $S_0$ - $S_1$ transition. The $S_2$ and $S_3$ states are now nearly isoenergetic with one another at the ground state geometry, lying 1.31 eV and 1.34 eV above $S_1$. Interestingly, the $S_0$-$S_2$ and $S_0$-$S_3$ electronic transitions now involve both $n\pi^*$ and $\pi\pi^*$ single electron transitions. The MOs associated with these transitions are shown in supplementary material (**Section S10**). Despite these differences, the large energy separation of $S_1$ from $S_2$/$S_3$ and smaller oscillator strength makes it unlikely that vibronic coupling will be manifested in the $S_0$-$S_1$ vibronic spectrum of the complex.

### 2. UV Excitation Spectroscopy

The labelled IR-UV HB spectrum of MA-$H_2O$ is shown in **Figure 12**. The spectrum spans from 28,500 - 30,000 $cm^{-1}$, with the $S_0$ - $S_1$ electronic origin transition appearing at 28,574 $cm^{-1}$, shifted 278 $cm^{-1}$ to the red of the MA monomer origin due to the relative water binding energies in the $S_0$ and $S_1$ states. The lifetime of the $S_1$ state is measured to be 23 ns, very close to that of the monomer (see **Figure S8b** for the fluorescence decay trace). The MA-$H_2O$ assignments included in **Figure 12** were reached based on corroborating evidence from $S_0$ and $S_1$ vibrational frequency calculations, zero-point energy calculations, excitation and DFL spectra (discussed below). Progressions in modes $\nu_{56}$ (187 $cm^{-1}$) and $\nu_{49}$ (427 $cm^{-1}$) are displayed via dotted tie-lines, while combination bands built off of $49^1_0$ are shown with solid tie-lines. All other assigned peaks are labelled with tags.

The Franck-Condon activity present in **Figure 12** bears some resemblance to that in MA monomer, most notably in the progressions of $\nu_{56}$ and $\nu_{49}$, which have their corresponding modes at similar frequencies in MA monomer ($\nu_{36}$, 179 $cm^{-1}$ and $\nu_{33}$, 421 $cm^{-1}$, respectively). **Table 2** lists the experimental and calculated MA-$H_2O$ $S_0$ and $S_1$ vibrational frequencies, along with their corresponding MA values. We note the presence of several analogous MA Franck-Condon active modes in the vibronic spectra of MA-$H_2O$. In many cases the frequencies increase in the presence of $H_2O$, indicating some stiffening of these in-plane vibrations (shown in **Figure S18**) when $H_2O$ is present.

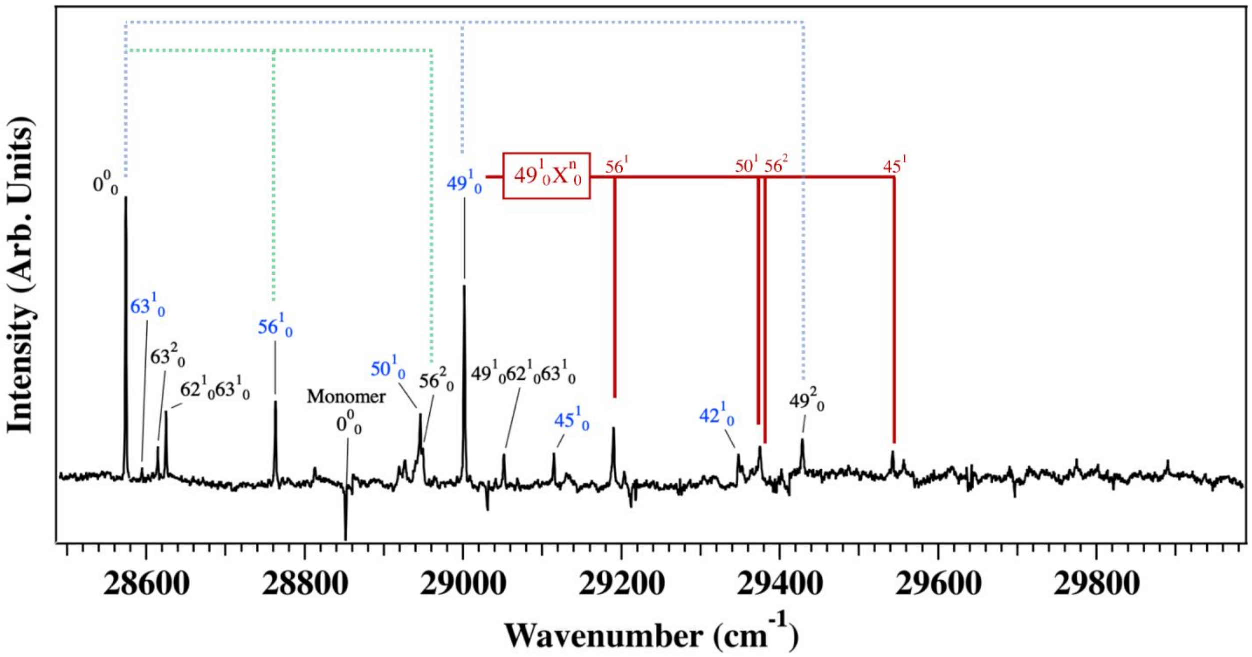

**Figure 12:** Assigned $S_0$ - $S_1$ LIF excitation spectrum of MA-$H_2O$. Progressions in the in-plane modes $\nu_{56}$ (189 cm$^{-1}$), and $\nu_{49}$ (427 cm$^{-1}$) are displayed via green and blue dotted tie-lines, respectively, while in-plane combination bands built off $49^1_0$ are shown with solid tie lines. The identity of mode X is listed above each respective tie line.

The triad of peaks immediately after the origin transition show an interesting intensity pattern, with each member of the triad more intense as frequency increases. If in both electronic states the geometry of MA-$H_2O$ is non-planar, then one might expect to see large Franck-Condon activity in modes with mostly out-of-plane character. Instead, what we observe is the overtone of $\nu_{63}$ ($63^2_0$) being three times as intense as its fundamental transition ($63^1_0$), and the $62^1_0 63^1_0$ combination band twice again as intense as the $63^2_0$ overtone. Both mode 62 and 63 are primarily intermolecular vibrations of the $H_2O$ molecule, with $\nu_{63}$ mostly an out-of-plane motion (see **Figure S18)**. These relative intensities suggest that the MA-$H_2O$ complex retains a weakened form of its $C_s$ selection rules in the complex; not surprisingly so, given that the electronic transition is localized on the planar MA monomer. As a result, the even overtone and 1+1 combination band are favored over the $63^1_0$ out-of-plane intermolecular fundamental.

### 3. Origin DFL Spectrum

The assigned DFL spectrum of the $0^0_0$ transition of MA-$H_2O$ is shown in **Figure 13**. As with MA, this spectrum generally mirrors that of the MA-$H_2O$ excitation spectrum, reflecting that Franck-Condon factors between the $S_0$ and $S_1$ electronic states of MA largely dictate the vibronic structure in both excitation and emission. The same two modes that were Franck-Condon active in the excitation spectrum, $\nu_{56}$ and $\nu_{49}$, also appear as progressions in the DFL spectrum. Mode 49 is also an active member in combination band transitions.

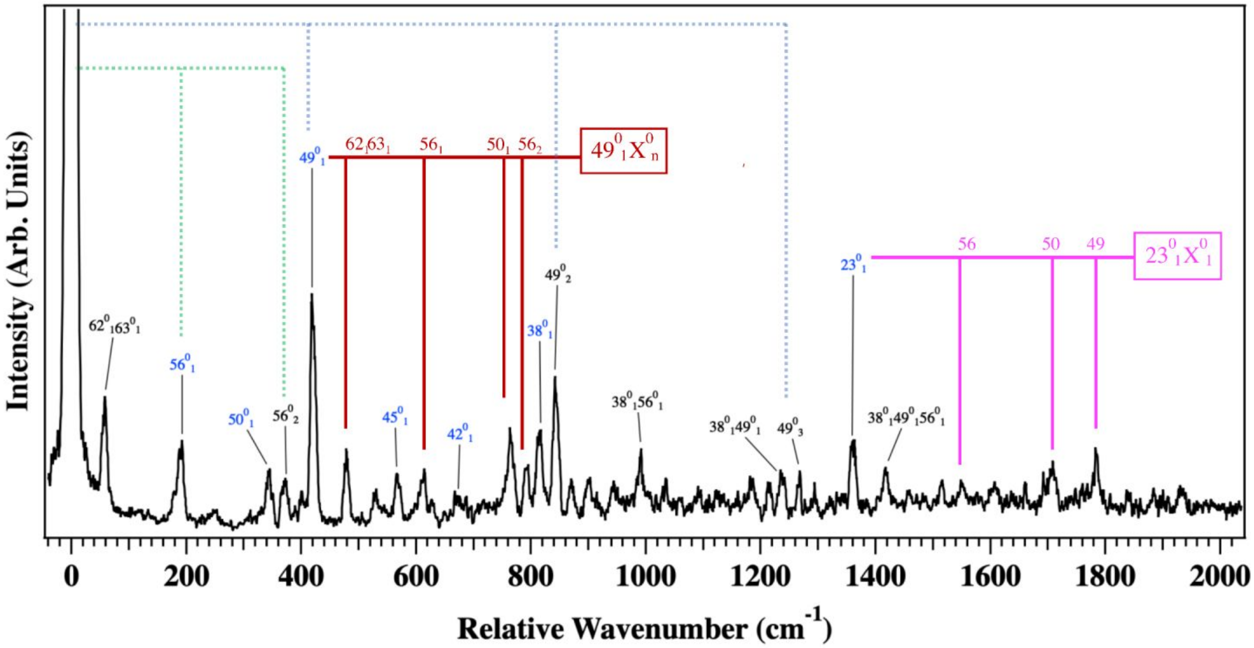

**Figure 13:** Dispersed fluorescence spectrum of the $S_0$ - $S_1$ origin transition of MA-$H_2O$. Progressions in the in-plane modes $\nu_{56}$ (187 cm$^{-1}$) and $\nu_{49}$ (418 cm$^{-1}$) are displayed via green and blue dotted tie-lines, respectively, while in-plane combination bands built off $49^0{}_1$ and $23^0{}_1$ are shown with solid tie lines. The identity of mode X is listed above each respective tie line.

The low frequency $62^0{}_163^0{}_1$ combination band at 58 cm$^{-1}$ in the $0^0$ DFL spectrum is the analogous combination band transition that we observed in the excitation spectrum ($62^1{}_063^1{}_0$). Due to the presence of intense laser scatter, we are not able to see whether this DFL spectrum contains the analogous $63^0{}_1$ and $63^0{}_2$ transitions that appeared in the excitation spectrum. It is worth noting that the ground state modes 62 and 63 are substantially mixed with one another in $S_1$, as revealed by large off-diagonal components in the Duschinsky matrix (see **Figure S18**). Several of the modes present in the excitation spectrum appears in the DFL spectrum with analogous Δv=1 transitions. Similarly, one higher frequency band is present in the DFL spectrum, $\nu_{23}$, appearing at 1363 cm$^{-1}$. This mode is analogous to $\nu_{18}$ in MA (see **Table 2**).

**Table 2: Experimental and Calculated $S_0$ and $S_1$ Frequencies of MA-$H_2O$[a]**

| | $S_0$ | | $S_1$ | |
|---|---|---|---|---|
| Mode | Exp Freq ($cm^{-1}$) | Calc Freq[b] ($cm^{-1}$) | Exp Freq ($cm^{-1}$) | Calc Freq[b] ($cm^{-1}$) |
| 63 | 9 | 10 | 20 | 22 |
| 62 | 49 | 50 | 31 | 33 |
| 56 (36) | 187 (179) | 185 | 189 (179) | 189 |
| 50 (34) | 345 (361) | 360 | 372 (366) | 362 |
| 49 (33) | 418 (412) | 428 | 427 (421) | 426 |
| 45 (31) | 568 (567) | 573 | 541 (540) | 560 |
| 42 (30) | 667 (672) | 684 | 773 (610) | 789 |
| 38 (29) | 817 (808) | 821 | - (773) | 789 |
| 23 (18) | 1363 (1355) | 1355 | - | 1382 |

[a] values in parentheses are analogous values of MA. [b] Frequencies calculated at the DFT B3LYP-D3BJ/def2TZVP level of theory.

## IV. Discussion

### A. Structural Changes Associated with Hydrogen Atom Dislocation

The Franck-Condon activity in several in-plane modes in the excitation and DFL spectra of MA indicate that the molecular geometries in the $S_0$ and $S_1$ states differ substantially from one another along these coordinates. We have carried out a near-complete assignment of the vibrationally-resolved LIF excitation scan and an array of DFL spectra out of single vibronic levels in the excited state. In all cases, the unscaled harmonic vibrational frequencies predicted by the DFT and TDDFT calculations at the B3LYP-D3BJ/def2TZVP level of theory closely reproduce the experimental values, with an average error of ±10.5 $cm^{-1}$. Furthermore, the rotational constants and transition dipole moment direction from calculation faithfully reproduce the rotational band contour of the electronic origin without adjustment. This leads to the conclusion that the calculations faithfully reproduce the ground state and excited state potential energy surfaces around the $S_0$ and $S_1$ minima, and therefore are anticipated to be trustworthy in the more detailed structural changes accompanying electronic excitation.

From an experimental viewpoint, while all the low-frequency in-plane vibrations have some Franck-Condon activity, longer progressions extending to v'=3 in modes 36 and 33, and v'=2 in mode 34 are evident in the $0^0$ DFL spectrum (**Figure 5**), reflecting largest geometry changes along these vibrational coordinates. Indeed, the majority of the vibronic structure in the excitation and DFL spectra can be accounted for as progressions and combination bands involving these three modes. These three modes all involve substantial in-plane motion of the $NH_2$ and $CO_2Me$ groups relative to one another. These heavy atom motions modulate the average distance between the H-bonded NH donor and the carbonyl oxygen acceptor groups along what might be termed the 'reaction coordinate' for a hydrogen atom transfer or dislocation. In a separate paper, we will view these effects on the interactions between the NH and C=O groups more directly by presenting infrared spectra of MA and MA-$H_2O$ in the NH stretch, NH bend, and C=O stretch regions in both $S_0$ and $S_1$ states.[33]

The low-frequency Franck-Condon activity that is the subject of the present work gives insight principally on the heavy atom motions that accompany electronic excitation. MA affords the opportunity to view this structural change by projecting a range of excited state vibrational levels back onto the ground state via their dispersed emission. As a result, armed with a comprehensive assignment of the electronic spectra, we now turn to a more detailed discussion of the structural change associated with the $\pi\pi^*$ electronic excitation, based on the optimized geometries shown in **Figure 2**.

In MA, the optimized ground state geometry has as its most characteristic feature the intramolecular H-bond between the $NH_2$ and C=O groups, with a H-bond distance of 1.926 Å associated with a short, but bent H-bond. This places the $NH_2$ group in an unusual situation in that amines are known most for their role as good H-bond acceptors due to the lone pair on the N atom, not as H-bond donors. Nevertheless, in the ground state, the structural effects of the NH···O=C H-bond are modest, with neither the NH nor C=O bond lengths being changed significantly from their ground state bond values in the singly-substituted analogs aniline ($NH_2$ only, $\Delta R$=+.001 Å) or methyl benzoate (methyl ester only, $\Delta R$=+0.012 Å), both of which lack the intramolecular H-bond. **Sections S12** and **S13** show calculated $S_0$ and $S_1$ structures of aniline and methyl benzoate.

The structural changes associated with electronic excitation are more dramatic. The primary changes involve structural distortions and positional changes in the $NH_2$ group relative to the methyl ester. First, the N-$H_{donor}$ and O=C bonds each increase in length by ~0.03 Å, characteristic changes associated with strengthening a H-bond between them. Second, the NH bond rotates towards the carbonyl oxygen, closing the CNH bond angle by 2°. Third, the CCN bond angle decreases from 122° to 116°. Taken together, these structural changes tilt and stretch the $NH_2$ group toward the methyl ester, contracting the 6-membered (C6) ring that is closed by the NH···O=C hydrogen bond. This results in a substantial decrease of the H···O hydrogen bonding distance by 0.203 Å, taking what is already a short H-bond ($R_{H...O}$ = 1.926 Å) and making it extraordinarily short ($R_{H...O}$ = 1.723 Å). Nearly identical structural changes occur in MA-$H_2O$ upon electronic excitation. One interesting difference, however, is that the H···O distance decreases by 0.02 Å less in MA-$H_2O$ than in MA. This is likely a result of the electronegative C=O oxygen acting as H-bond acceptor to both the NH and water OH, thereby decreasing its affinity for the dislocated NH. **Table 3** lists the $S_0$, $S_1$, and difference in structural parameters for MA and MA-$H_2O$.

In previous work on anthranilic acid, the excited state structural change was labeled as a 'hydrogen-atom dislocation' to indicate its partial nature, as distinct from 'hydrogen-atom transfer', in which a hydrogen atom is completely transferred from one nucleus to another.[15] For further comparison of the anthranilates upon electron excitation, see **Section S14**. As we will discuss in more detail in the following section, in salicylic acid and similar molecules, the transfer involves O-H bond lengthening, with relaxation along several heavy-atoms on the $S_1$ potential energy surface and subsequent red-shifted emission and/or non-radiative decay via an $S_1/S_0$ conical intersection (CI).[2-4, 12] In MA, we have investigated the $S_0$-$S_1$ Franck-Condon active region, and see no evidence of hydrogen atom transfer near the $S_1$ origin. This is demonstrated by the absence of non-radiative processes in the UV-D spectrum, and the lack of strongly red-shifted emission in the DFL spectra.

What the present study has achieved is a deeper understanding of what 'hydrogen atom dislocation' means in methyl anthranilate. As just summarized, the optimized excited state structure has an H···O distance 0.203 Å shorter than in the ground state, with $R_{H...O}$=1.723 Å. If full transfer were to shorten this distance to 1.0 Å, then the dislocation in MA is about 25% of full transfer. However, only 0.03 Å of this dislocation involves lengthening the NH bond, while the remaining 0.173 Å is due to the heavy atom motion just described that reorients the entire $NH_2$ group relative to the C=O acceptor. Further details of the Franck-Condon analysis involving vibrational motions of the $NH_2$ and COOMe is included in supplementary material (**Section S15**).

**Table 3: Structural Parameters of MA and MA-$H_2O$[a]**

| | Methyl Anthranilate | | | Methyl Anthranilate:$H_2O$ | | |
|---|---|---|---|---|---|---|
| | $S_0$ | $S_1$ | Δ | $S_0$ | $S_1$ | Δ |
| $R_{C\text{-}N}$[b] | 1.359 | 1.356 | -0.003 | 1.360 | 1.355 | -0.005 |
| $R_{N\text{-}Hdonor}$ | 1.008 | 1.035 | 0.027 | 1.008 | 1.030 | 0.022 |
| $R_{N\text{-}Hfree}$ | 1.003 | 1.007 | 0.004 | 1.003 | 1.007 | 0.004 |
| $\theta_{H\text{-}N\text{-}H}$[c] | 120° | 124° | 4° | 120° | 123° | 3° |
| $D_{CNHH}$ | 0° | 0° | 0° | 11° | 3° | -8° |
| $R_{C=O}$ | 1.220 | 1.252 | 0.032 | 1.227 | 1.261 | 0.034 |
| $R_{C\text{-}O}$ | 1.349 | 1.364 | 0.015 | 1.338 | 1.357 | 0.019 |
| $\theta_{O=C\text{-}O}$ | 121 | 121° | 0° | 122° | 121° | -1° |
| $R_{H\cdots O}$ | 1.926 | 1.723 | -0.203 | 1.935 | 1.755 | -0.180 |
| $\theta_{N\text{-}Hdonor\text{-}O}$ | 130° | 141° | 11° | 129° | 139° | 10° |
| $R_{OH\text{-}O}$ | -- | -- | -- | 1.910 | 1.830 | -0.080 |
| $R_{HO\text{-}C}$ | -- | -- | -- | 3.317 | 3.537 | 0.220 |
| $\theta_{O\text{-}H\cdot\cdot O}$ | -- | -- | -- | 171° | 178° | 7° |

[a]Structures calculated at the DFT B3LYP-D3BJ/def2TZVP level of theory.

[b] Distances in Å. [c]Angles in degrees.

### B. Photophysical Properties of MA and Implications as a Sunscreen Precursor

MA is the precursor to menthyl anthranilate (MenA), an FDA approved sunscreen agent. Rodrigues *et al.* have recently shown, in both condensed- and gas-phase, that MA and MenA exhibit nearly identical photochemical/photophysical properties.[13] In order to put the absorption and photophysical properties of MA in proper context, we compare MA first to its simpler analogs, aniline ($NH_2$ substitution only) and methyl benzoate ($CO_2Me$ substitution only).

Aniline is a prototypical aromatic amine that has been studied extensively. Its $S_0$-$S_1$ origin appears at 34,025 $cm^{-1}$, and is readily detected by both fluorescence and R2PI schemes.[34-38] Using the same level of theory as in MA, we calculated $S_0$ and $S_1$ state optimized geometries for aniline (shown in **Figure S19**). The $S_0$-$S_1$ transition of aniline is a prototypical $\pi\pi^*$ transition for a phenyl derivative, leading to expansion in the size of the aromatic ring, modest shortening of the CN bond ($\Delta R_{CN}$ = -0.026 Å), and planarization of the $NH_2$ group in the $S_1$ state.

Methyl benzoate (MB), by contrast, has its $S_0$-$S_2$ transition (the first optically accessible singlet $\pi\pi^*$ state, see **Section S13**) at 36,105 $cm^{-1}$, but cannot be detected either in LIF or R2PI due to fast intersystem crossing (ISC) to the $n\pi^*$ triplet state that shortens the excited state lifetime and reduces the fluorescence quantum yield. Its spectroscopy has been studied using sensitized phosphorescence detection.[39] **Table 4** shows the energetic ordering of electronic states of aniline, MB, MA, and MA-$H_2O$. The calculated structural changes associated with electronic excitation (shown in **Figure S20**) include expansion in the size of the aromatic ring, substantial lengthening of the C=O bond ($\Delta R_{C=O} = +0.110$ Å) and a closing of the O=C-O angle ($\Delta\theta_{O=C-O} = -10°$).

**Table 4: Electronic States in Aniline, Methyl Benzoate, Methyl Anthranilate, and Methyl Anthranilate-$H_2O$[a]**

| Aniline | | | Methyl Benzoate | | | Methyl Anthranilate | | | Methyl Anthranilate-$H_2O$ | | |
|---|---|---|---|---|---|---|---|---|---|---|---|
| State | Energy (ev) | $f_{0n}$ | State | Energy (eV) | $f_{0n}$ | State | Energy (eV) | $f_{0n}$ | State | Energy (eV) | $f_{0n}$ |
| $^3\pi\pi^*$ | 3.65 | 0.0000 | $^3\pi\pi^*$ | 3.57 | 0.0000 | $^3\pi\pi^*$ | 3.03 | 0.0000 | $^3\pi\pi^*$ | 2.95 | 0.0000 |
| $^3\pi\pi^*$ | 3.86 | 0.0000 | $^3\pi\pi^*$ | 4.18 | 0.0000 | $^3\pi\pi^*$ | 3.56 | 0.0000 | $^3\pi\pi^*$ | 3.50 | 0.0000 |
| $^3\pi\pi^*$ | 4.49 | 0.0000 | $^3n\pi^*$ | 4.47 | 0.0000 | $^1\pi\pi^*$ | 3.92 | 0.1036 | $^1\pi\pi^*$ | 3.84 | 0.1077 |
| $^1\pi\pi^*$ | 4.75 | 0.0359 | $^3\pi\pi^*$ | 4.53 | 0.0000 | $^3\pi\pi^*$ | 4.17 | 0.0000 | $^3\pi\pi^*$ | 4.12 | 0.0000 |
| $^3\pi\pi^*$ | 5.32 | 0.0000 | $^1n\pi^*$ | 4.88 | 0.0001 | $^3n\pi^*$ | 4.69 | 0.0000 | $^3n\pi^*$ | 4.81 | 0.0000 |
| $^3\pi\pi^*$ | 5.40 | 0.0000 | $^1\pi\pi^*$ | 4.97 | 0.0153 | $^1n\pi^*$ | 5.08 | 0.0002 | $^1n\pi^*/\pi\pi^*$ | 5.15 | 0.0530 |
| $^1\pi\pi^*$ | 5.42 | 0.0644 | $^3\pi\pi^*$ | 5.07 | 0.0000 | $^1\pi\pi^*$ | 5.23 | 0.0481 | $^1n\pi^*/\pi\pi^*$ | 5.18 | 0.0117 |

[a] Values calculated at the DFT B3LYP-D3BJ/def2TZVP level of theory

Inclusion of both methoxycarbonyl and amine groups as *ortho*-ring substituents in MA modifies the properties of the singly-substituted molecules in several ways. The absorbing states are redshifted from the UV-B (280 - 315 nm) region (276.9 nm in MB and 293.9 nm in aniline) into the UV-A region (315 - 400 nm), with $S_0$-$S_1$ origin at 346.9 nm and low-frequency Franck-Condon activity stretching to 333.3 nm in the gas phase (see **Figure 14** for the molecular orbitals involved in the $S_0$ - $S_1$ transitions in MA). The TDM vectors of the bright transitions of MB and Aniline essentially add to form the TDM vector in MA, with the oscillator strength of the MA nearly tripling that of aniline and increasing by nearly an order of magnitude in MB, respectively (see **Figure S25**).

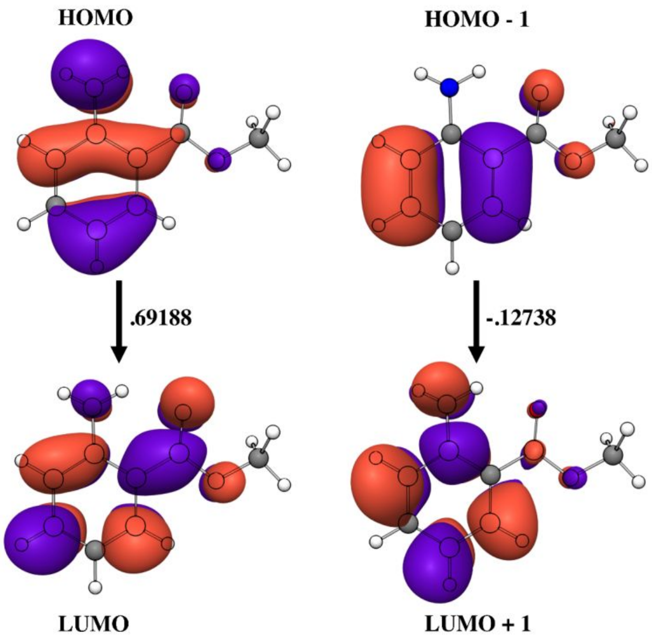

**Figure 14:** Molecular orbitals (MO) transitions comprising the $S_0$ - $S_1$ transition of MA, along with their coefficients. Additional MOs of molecules discussed herein are presented in the supporting information. Calculations were carried out at the DFT B3LYP-D3BJ/def2TZVP level of theory.

Relative to MB, MA's inclusion of the amine group reorders the electronic states substantially. In MB, the ester C=O group gives rise to a triplet nπ* state that, according to calculations, lies 4,033 $cm^{-1}$ (0.5 eV) below the absorbing singlet ππ* state (see **Table 4**). In accordance with El-Sayed's rule, $^1\pi\pi^* \leftrightarrow {}^3n\pi^*$ ISC is efficient when energetically allowed, producing an experimentally observed long-lived non-fluorescent state.[39] The strong intramolecular hydrogen bond in MA, which includes bonding of the C=O lone electron pair, results in an increase in energy of the nπ* state relative to the ππ* state. According to calculations, this raises the energy of the triplet nπ* state to 6,210 $cm^{-1}$ (0.77 eV) above that of the absorbing singlet ππ* state. The destabilization of the triplet nπ* state in MA removes the possibility of ISC involving that state.

The lack of formation of long-lived, reactive, triplet state species upon photoexcitation of MA is in accordance with its having the same electronic chromophore as active sunscreen agents. On the other hand, effective sunscreens typically undergo efficient non-radiative decay from the excited state back to the ground state, thereby recycling their UV-absorption capacity. In several of these molecules, excited-state deactivation is thought to be facilitated by H-atom transfer on the $S_1$ surface[3, 4, 40], in some cases followed by transient C=C bond rotation, at which geometries the $S_1$ and $S_0$ surfaces meet at a conical intersection.[5-7, 40-42] Internal conversion, accompanied by hydrogen atom back-transfer, restores the molecule to the ground electronic state configuration. Alternatively, as is thought to be the case with salicylic acid and methyl salicylate, the H-atom transferred excited state may become trapped in a local minimum on the $S_1$ surface, resulting in Stokes-shifted emission. [3, 4, 9, 10]

Our characterization of the excited state of MA agrees with results from a recent time-domain study of MA by Rodriguez *et al.* where they presented experimental and computational evidence indicating that a complete hydrogen atom transfer from a region near the $S_1$ origin is endothermic.[13] These authors computed a two-step, endothermic (no bound intermediates) pathway toward a conical intersection, involving motion along a 1700 cm$^{-1}$ barrier to an unbound hydrogen atom transfer geometry followed by a 3200 cm$^{-1}$ barrier to ester group (C=C) rotation, at which geometry $S_1$ and $S_0$ curves meet at a CI. In a follow up study, they observed damping of time-dependent quantum beat signals upon irradiation centered at 315 nm, at photoexcitation energies ~1,200 cm$^{-1}$ above the H-atom transfer barrier (2,000 cm$^{-1}$ below the CI barrier), which they attributed to the rapid redistribution of energy via IVR.[43] This is in good agreement with our observation of broadened DFL scans occurring in the excited state of MA with only ~800 cm$^{-1}$ excess energy, at which the density of $S_1$ vibrational states is calculated to be 14 states/cm$^{-1}$.[43] Their time- and our frequency-resolved data indicate that, in the $S_0$-$S_1$ Franck-Condon active region, while the structural changes associated with electronic excitation would seem to facilitate H-atom transfer, there exists no bound intermediate on the excited state surface on which the tautomer product can exist. Taken as a whole, the excited state properties of methyl anthranilate near the $S_0$-$S_1$ origin show no fast non-radiative pathways that one typically associates with efficient sunscreens. The same is likely true of menthyl anthranilate, bolstering the case for rational sunscreen design.

## V. Conclusion

We have presented the LIF excitation and dispersed fluorescence spectra of methyl anthranilate, leading to assignment of nearly every vibronic transition in the first ~1,000 cm$^{-1}$ of the excitation and DFL spectra. The observed transitions prove that MA retains $C_s$ symmetry in both its $S_0$ and $S_1$ states. The presence of cross-sequence bands in the DFL spectra of MA indicate a high degree of Duschinsky mixing between $S_0$ and $S_1$ states involving both out-of-plane and in-plane normal modes. The presence of so many in-plane normal modes in the vibronic spectra indicate a displacement of their respective normal mode coordinates upon electronic excitation, and reflect a significant change in geometry upon electronic excitation. More importantly, the spectrum is dominated by Franck-Condon progressions involving three low-frequency in-plane modes ($\nu_{33}$, $\nu_{34}$, and $\nu_{36}$) that modulate the distance between the $NH_2$ and $CO_2Me$ groups during their vibrational motion.

A combination of experimental and corroborating computational evidence provides a more detailed picture of this structural change, identifying it as a rocking and re-orientation of the $NH_2$ and $CO_2Me$ groups that brings them closer to one another, thereby strengthening the six-membered hydrogen bonded ring between the two groups. In particular, upon electronic excitation, the H···O hydrogen bonding distance decreases by 0.203 Å to a value of just 1.723 Å. Since a full H-atom transfer would result in an O-H bond of about 1.0 Å, the 0.20 Å shortening is aptly labeled as a hydrogen-atom dislocation, although it is largely the heavy atoms that rearrange to close the transfer distance, since the N-$H_{donor}$ bond distance increases by only 0.027 Å. At the same time, the process is far short of a complete hydrogen atom transfer. Indeed, as the UV-D and DFL spectra indicate, in the Franck-Condon active region, the changes in MA associated with electronic excitation are primarily structural and not non-radiative.

We have also presented LIF excitation and $0^0_0$ DFL spectra for the MA-$H_2O$ complex. In the assigned structure, the water molecule hydrogen bonds to the 'back side' of the C=O group weakening but not disrupting the intramolecular NH···O=C H-bond. As a result, much of the Franck-Condon activity associated with the electronic transition is retained in the complex.

While this paper has focused attention on the electronic spectroscopy of MA and MA-$H_2O$, infrared spectroscopy can provide a complementary probe of the pre-reactive structural changes. In fact, the NH, OH, and C=O oscillators serve as sensitive reporters of their local environments. In an upcoming paper, we build upon our results here by reporting on the hydride stretch and mid-infrared spectra of MA and MA-$H_2O$ in both ground and excited states.

## Conflicts of Interest

There are no conflicts to declare.

## Acknowledgements

KNB, DS, JLF, and TSZ gratefully acknowledge support for this work from the National Science Foundation under grant NSF-CHE1764148. ELS acknowledge support from the National Science Foundation under grant NSF-CHE-1566108.

## References

1. A. Beeby and A. E. Jones, *Photochem. Photobiol.*, 2000, **72**, 10-15.
2. T. N. V. Karsili, B. Marchetti, M. N. R. Ashfold and W. Domcke, *J. Phys. Chem. A*, 2014, **118**, 11999-12010.
3. A. L. Sobolewski and W. Domcke, *PCCP*, 2006, **8**, 3410-3417.
4. P. B. Bisht, H. Petek, K. Yoshihara and U. Nagashima, *J. Chem. Phys.*, 1995, **103**, 5290-5307.
5. Y. Peperstraete, M. Staniforth, L. A. Baker, N. D. N. Rodrigues, N. C. Cole-Filipiak, W.-D. Quan and V. G. Stavros, *PCCP*, 2016, **18**, 28140-28149.
6. L. A. Baker, M. D. Horbury, S. E. Greenough, P. M. Coulter, T. N. Karsili, G. M. Roberts, A. J. Orr-Ewing, M. N. Ashfold and V. G. Stavros, *J. Phys. Chem. L.*, 2015, **6**, 1363-1368.
7. N. D. Rodrigues, M. Staniforth and V. G. Stavros, *Proceedings of the Royal Society A: Mathematical, Physical and Engineering Sciences*, 2016, **472**, 20160677.
8. L. A. Baker, B. Marchetti, T. N. Karsili, V. G. Stavros and M. N. Ashfold, *Chem. Soc. Rev.*, 2017, **46**, 3770-3791.
9. L. Heimbrook, J. E. Kenny, B. E. Kohler and G. W. Scott, *The Journal of Physical Chemistry*, 1983, **87**, 280-289.
10. L. A. Heimbrook, J. E. Kenny, B. E. Kohler and G. W. Scott, *J. Chem. Phys.*, 1981, **75**, 5201-5203.
11. J. Zhao, S. Ji, Y. Chen, H. Guo and P. Yang, *PCCP*, 2012, **14**, 8803-8817.
12. T. Raeker and B. Hartke, *J. Phys. Chem. A*, 2017, **121**, 5967-5977.
13. N. D. N. Rodrigues, N. C. Cole-Filipiak, M. D. Horbury, M. Staniforth, T. N. V. Karsili, Y. Peperstraete and V. G. Stavros, *J. Photochem. Photobiol. A: Chem.*, 2018, **353**, 376-384.
14. J. A. Stearns, A. Das and T. S. Zwier, *PCCP*, 2004, **6**, 2605-2610.
15. C. A. Southern, D. H. Levy, G. M. Florio, A. Longarte and T. S. Zwier, *J. Phys. Chem. A*, 2003, **107**, 4032-4040.
16. A. L. Sobolewski and W. Domcke, *J. Phys. Chem. A*, 2004, **108**, 10917-10922.
17. E. A. E.-H. Abou El-Nasr, A. Fujii, T. Yahagi, T. Ebata and N. Mikami, *J. Phys. Chem. A*, 2005, **109**, 2498-2504.
18. S. Leśniewski, P. Kolek, K. Pirowska, A. L. Sobolewski and J. Najbar, *J. Chem. Phys.*, 2009, **130**, 054307.
19. P. Kolek, M. Andrzejak, R. Hakalla and W. Szajna, *J. Phys. Chem. A*, 2018, **122**, 6243-6255.
20. N. R. Pillsbury, C. W. Muller, W. L. Meerts, D. F. Plusquellic and T. S. Zwier, *J. Phys. Chem. A*, 2009, **113**, 5000-5012.

21. S. Grimme, *J. Comput. Chem.*, 2004, **25**, 1463-1473.
22. S. Grimme, *J. Chem. Phys.*, 2006, **124**, 034108.
23. M. Frisch, G. Trucks, H. Schlegel, G. Scuseria, M. Robb, J. Cheeseman, G. Scalmani, V. Barone, G. Petersson and H. Nakatsuji, *Revision A*, 2016, **3**.
24. G. Zhurko and D. Zhurko, *URL: http://www.chemcraftprog.com*, 2009.
25. P. Butler, D. B. Moss, H. Yin, T. W. Schmidt and S. H. Kable, *J. Chem. Phys.*, 2007, **127**, 094303.
26. R. S. Mulliken, *J. Chem. Phys.*, 1955, **23**, 1997-2011.
27. D. F. Plusquellic, R. Suenram, B. Mate, J. Jensen and A. Samuels, *J. Chem. Phys.*, 2001, **115**, 3057-3067.
28. F. Duschinsky, *Acta Physicochim. URSS*, 1937, **7**, 551-566.
29. C. W. Muller, J. J. Newby, C.-P. Liu, C. P. Rodrigo and T. S. Zwier, *PCCP*, 2010, **12**, 2331-2343.
30. J. B. Hopkins, D. E. Powers and R. E. Smalley, *J. Chem. Phys.*, 1980, **72**, 5039-5048.
31. J. B. Hopkins, D. E. Powers, S. Mukamel and R. E. Smalley, *J. Chem. Phys.*, 1980, **72**, 5049-5061.
32. C.-P. Liu, J. J. Newby, C. W. Müller, H. D. Lee and T. S. Zwier, *J. Phys. Chem. A*, 2008, **112**, 9454-9466.
33. K. N. Blodgett, J. L. Fischer, D. Sun, E. L. Sibert III and T. S. Zwier, *Manuscript In Preparation*, 2019.
34. N. Mikami, A. Hiraya, I. Fujiwara and M. Ito, *Chem. Phys. Lett.*, 1980, **74**, 531-535.
35. M. Quack and M. Stockburger, *J. Mol. Spectrosc.*, 1972, **43**, 87-116.
36. E. R. T. Kerstel, M. Becucci, G. Pietraperzia, D. Consalvo and E. Castellucci, *J. Mol. Spectrosc.*, 1996, **177**, 74-78.
37. J. H. Brophy and C. T. Rettner, *Chem. Phys. Lett.*, 1979, **67**, 351-355.
38. J. T. Meek, E. Sekreta, W. Wilson, K. Viswanathan and J. P. Reilly, *J. Chem. Phys.*, 1985, **82**, 1741-1749.
39. S. Kamei, H. Abe, N. Mikami and M. Ito, *The Journal of Physical Chemistry*, 1985, **89**, 3636-3641.
40. T. N. Karsili, B. Marchetti, M. N. Ashfold and W. Domcke, *J. Phys. Chem. A*, 2014, **118**, 11999-12010.
41. K. Yamazaki, Y. Miyazaki, Y. Harabuchi, T. Taketsugu, S. Maeda, Y. Inokuchi, S.-n. Kinoshita, M. Sumida, Y. Onitsuka and H. Kohguchi, *J. Phys. Chem. L.*, 2016, **7**, 4001-4007.
42. S.-n. Kinoshita, Y. Miyazaki, M. Sumida, Y. Onitsuka, H. Kohguchi, Y. Inokuchi, N. Akai, T. Shiraogawa, M. Ehara and K. Yamazaki, *PCCP*, 2018, **20**, 17583-17598.
43. N. d. N. Rodrigues, N. C. Cole-Filipiak, K. N. Blodgett, C. Abeysekera, T. S. Zwier and V. G. Stavros, *Nature Communications*, 2018, **9**, 5188.

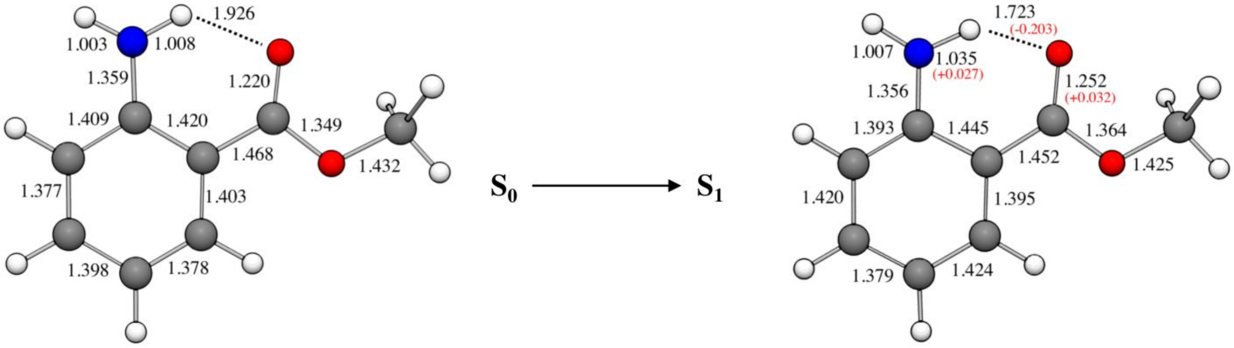

Hydrogen atom dislocation in the $S_1$ state of methyl anthranilate and its water complex is characterized using vibronic spectroscopy.